Journal of Alloys and Compounds 591 (2014) 362–369

Contents lists available at ScienceDirect

Journal of Alloys and Compounds

journal homepage: www.elsevier.com/locate/jalcom

Electronic structure, optical and thermoelectric transport properties of layered polyanionic hydrosulfate $LiFeSO_4OH$: Electrode for Li-ion batteries

A.H. Reshak [a,b], Wilayat Khan [a,*]

[a] New Technologies-Research Center, University of West Bohemia, Univerzitni 8, 306 14 Pilson, Czech Republic
[b] Center of Excellence Geopolymer and Green Technology, School of Material Engineering, University Malaysia Perlis, 01007 Kangar, Perlis, Malaysia

ARTICLE INFO

Article history:
Received 1 December 2013
Received in revised form 24 December 2013
Accepted 26 December 2013
Available online 7 January 2014

Keywords:
Electronic structure
Optical properties
Thermoelectric properties
Boltztrap code
EVGGA

ABSTRACT

Theoretical analysis of electronic structure and optical properties of $LiFeSO_4OH$, using the full-potential linearized augmented plane waves (FPLAPW), on the basis of density-functional theory (DFT), with in the local density approach (LDA), generalized gradient approach (GGA) and Engel–Vosko GGA (EVGGA). Electronic structure and bonding nature of the atoms are investigated in the entire calculation of partial, total density of states and electronic charge densities. The band structure calculations show that the investigated compound is direct band gap semiconductor of about 0.334 eV, 0.580 eV and 1.114 eV. The optical spectra are calculated using EVGGA in the photon energy range up to 13.8 eV. The anisotropic behavior of the imaginary and real parts of the complex dielectric function, reflectivity, refractive index, extension co-efficient and energy loss function are studied for parallel and perpendicular component of electric field polarization. Thermoelectric properties namely, electrical and thermal conductivity, Seebeck co-efficient and power factor are calculated and discussed with the constant relaxation time, using the BoltzTraP code.

1. Introduction

Li-ion batteries have dominated the whole world of conveniently transported electronics and are considered as the best foremost technologies to power electric vehicles. Even these Li-ion are used as a good materials in the area of renewable sources (wind and solar) for balancing recurrent with user requirements. On the other hand, intended for this technology to sustain such hefty-volume markets, endeavors must be engrossed on growing their energy density and slashing their costs, at the same time as concurrently tackling viability concerns. A substantial study has been stanched to surrogated layered oxides, which revealed the capabilities as lofty as 250 mA h/g for an average voltage of 3.8 V vs Li^+/Li [1]. Even as these layered oxides have a reasonable energy densities, it has great cost because of the transition metals (Co and Ni) and also due to the synthesis of active phases make them less viable for large-volume applications. On the other hand, many attempts are being intended for the development of Fe-based polyanionic compounds, for instance for $LiFePO_4$ [2], $Li_2FeSiSO_4$ [3], $Li_2FeP_2O_7$ [4], and $LiFeBO_3$ [5]. This has been found that the Fe-based compounds has the low-cost compensation owed to both the profusion of their component elements and the viability, in nearly all casing, by means of competent synthesis methods to set up them. Comparatively to the layered oxide materials, the Fe-based materials give much lower energy densities. Consequently, joining the electro negativity of fluorine and the inductive effect [6] improved by the company of a SO_4^{2-} polyanion in the structure, Subban et al. [16] urbanized a novel family of fluorosulfates of the general formula A_xMSO_4F, where A = Li, Na, K and M = 3d metals [7–15]. Among them, $LiFeSO_4F$ seems to be the mainly appealing on behalf of crystal chemistry and electrochemical performance. It is well-known that there are two polymorphs for $LiFeSO_4F$, these are tavorite and triplite, with redox potentials 3.6 and 3.9 Volts vs Li^+/Li^0, respectively [7,13,15]. $LiFeSO_4OH$ possess the highest Fe^{+3}/Fe^{+2} redox voltage among any inorganic compound. The triplite polymorphs of $LiFeSO_4F$ exhibit a theoretical energy density of about 577 W h/kg, in close agreement to that obtained from $LiFePO_4$ [16]. Moreover, Subban et al. [16] illustrated that this phase can be completed at room temperature via mechanochemical synthesis, which recommend simple scalability and small price preparation [11]. Subban et al. [16] report the preparation of these symmetries along with the tenacity of their crystal configuration and their characteristic (electrochemical). In addition, the author isolate transitional Li-free $M_3(SO_4)_2(OH)_2$ (M = Fe, Co, Mn and Ni) phase which carry the composition of $Mg_3(SO_4)_2(OH)_2$ (mineral caminite).

* Corresponding author. Tel.: +420 775526684.
E-mail address: walayat76@gmail.com (W. Khan).

0925-8388/$ - see front matter © 2014 Elsevier B.V. All rights reserved.
http://dx.doi.org/10.1016/j.jallcom.2013.12.232

2. Computational method

The first principle calculations reported in this article are executed within the Engel–Vosko GGA (EVGGA) [17] approximation, based on the density functional theory (DFT) [18–20] as employed in the WIEN2K computer package [21], using the full potential linearized augmented plane wave (FPLAPW) technique [22–28]. In the FPLAPW technique, the potential is expanded into lattice harmonics inside the individual sphere of atom of a compound as well as the charge density is expanded as a Fourier series inside the interstitial section. In this technique, the unit cell is separated into two parts: (1) non-overlapping atomic spheres and (2) an interstitial section. Using the high-resolution neutron powder diffraction data of $LiFeSO_4OH$ taken from Subban et al. [16], we have optimized the structure by minimizing the forces acting on each atom using EVGGA, these are presented in Table 1. The optimize structure of $LiFeSO_4OH$ compound is shown in Fig. 1. From the relaxed geometry we have calculated the electronic band structure, partial and total density of states, electronic charge density, optical and thermoelectric properties. In our calculation, we have used $R_{MT}K_{max} = 7$, the convergence parameter that assess the shape of the matrix. The maximum value of the angular quantum number inside the atomic region is $l_{max} = 10$. The self-consistent iterations are chosen to ensure the convergence of total energy within 10^{-3} mRy. For the structure properties of our investigated compound Li_2FeSO_4OH, we use the local density approach (LDA) [29], generalized gradient approach (GGA) [30] in the form of Perdew–Burke–Ernzerh (PBE) and Engel–Vosko GGA (EVGGA) approach.

Here in this work, we calculate electronic structure, opto-electrical properties i.e. dielectric function, reflectivity, energy loss function, absorption co-efficient, refractive index and extension co-efficient by means of ab initio total energy calculation based on the density functional theory (DFT), within the more exact all-electrons full potential technique. We also calculate and study thermoelectric properties as a function of carrier concentration at different temperatures using BoltzTraP code.

Table 1
Lattice constant and atomic positions of $LiFeSO_4OH$.

			Exp			Caltd
Lattice parameters						
a (Å)			9.5147			9.5147
b (Å)			5.5087			5.5087
c (Å)			7.3755			7.375
Atomic co-ordinates						
Atom	*x*	*y*	*z*	*x*	*y*	*z*
Fe	0.5551	0.2635	0.6261	0.5477	0.2621	0.6164
S	0.7922	0.5615	0.9853	0.7782	0.5568	0.9849
O	0.5733	0.4246	0.3739	0.5549	0.4235	0.3657
O	0.6490	0.9345	0.5328	0.6374	0.9403	0.5433
O	0.7647	0.0471	0.2989	0.7451	0.0631	0.2908
O	0.1566	0.1833	0.0162	0.1711	0.1885	0.0222
O	0.0954	0.9209	0.3656	0.1023	0.9158	0.3696
Li	0.0759	0.924	0.822	0.0865	0.9403	0.8186
H	0.3322	−0.0090	0.0932	0.3434	0.9864	0.1057

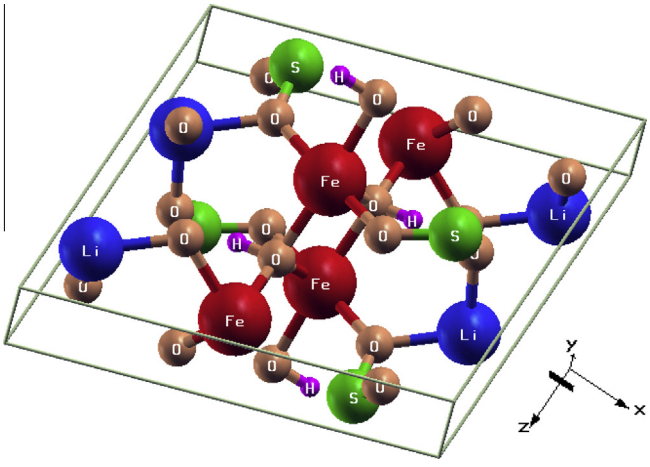

Fig. 1. Molecular structure of $LiFeSO_4OH$.

3. Result and discussion

3.1. Electronic structure

In Fig. 2(a–c), we displayed the dispersion of calculated electronic band structure (BS) of the layered polyanionic hydroxysulfate $LiFeSO_4OH$ along the high symmetry points in the irreducible Brillouin Zone (IBZ). The calculation show that the valence band maximum (VBM) and the conduction band minimum (CBM) are positioned at the G–Z-points of IBZ. Thus $LiFeSO_4OH$ is narrow direct band gap semiconductor. The value of the calculated band gap using LDA, GGA and EVGGA are displayed in Table 2. Following Table 2, the band gaps are analytically underestimated in first principle studies, and this is an intrinsic characteristic of the density functional theory (DFT), because DFT being a ground-state theory is not appropriate for explaining excited-state properties of the electronic system, such as the energy gap. Therefore, we preferred the EV – GGA correction which improves the band gap as compared to LDA and GGA, for further structural analysis of our investigated compound $LiFeSO_4OH$. The total density of states (TDOS) and partial density of states (PDOS) projected in lithium, iron, sulfur, oxygen and hydrogen atoms spheres and interstitial sections are shown in Fig. 3(a–d). Following this figure one can see that, the region from −14.0 eV to −12.0 eV is mainly covered by the s orbital (0.85 states/eV) of S atoms. The orbital p (1.8 states/eV) of S atom and orbital s (0.24 states/eV) of O atoms exhibit high contribution, while the orbital s (0.02 states/eV) of both H and Li atoms and s (0.04 states/eV) and p orbital (0.02 states/eV) of Fe atom posses small contribution to the PDOS in the energy range from −12.0 eV to −9.0 eV in the valence band (VB). In the energy region from −9.0 eV to −6.0 eV, the prominent contribution arise from the p orbital (2.24 states/eV) of O atoms, the small contribution appear due to s orbital (0.43 states/eV) of H atoms and orbital s (0.14 states/eV) of both Fe/S atoms, and negligible contribution from the s (0.01 states/eV), p (0.04 states/eV) orbitals of Li/Fe atoms is observed. In the second last part of the valence band (VB), which start from energy range −6.0 eV to −3.0 eV, the orbital p (1.7 states/eV) of O atoms and the orbital d (0.61 states/eV) of Fe atom indicate major support while the remaining display small contribution to this part of the valence band. The last part of the valence band which lies just below the Fermi level ranging from −3.0 eV to 0.0 eV, is supported strongly from the orbital d (11.15 states/eV) of Fe atoms and small support from p orbital (0.14 states/eV) of O atom and the rest for example s orbitals of H/Fe atoms and p orbital of Fe atom have negligible contribution to this portion of the valence band. From TDOS, one can note that the whole structure is shifted toward high energy as we move from LDA to GGA then EVGGA approaches, respectively as illustrated in Fig. 3a.

3.2. Electronic charge density

The electronic charge densities visualize the nature of the bond character, explaining the charge transfer and bonding properties of $LiFeSO_4OH$. The effect of each individual atom i.e. Li, Fe, S, O and H on the total electronic charge density is also studied. Fig. 4(a–c) indicates the 2D contour plot in the planes (110), (100) and (001) for the total electronic charge density of the compound $LiFeSO_4OH$. The Pauling electronegativity of the atoms Li, Fe, S, O and H are 0.98, 1.83, 2.58, 3.44 and 2.20, respectively. It is obvious from Fig. 4(a and b) that there is a covalent bonding between O and H/S atoms because of small electronegativity difference between them. The difference of the electronegativity between Fe and O atoms is (1.61) indicate the polar covalent bond. The electronegativity difference between O and Li atoms is greater (2.46), which depicts

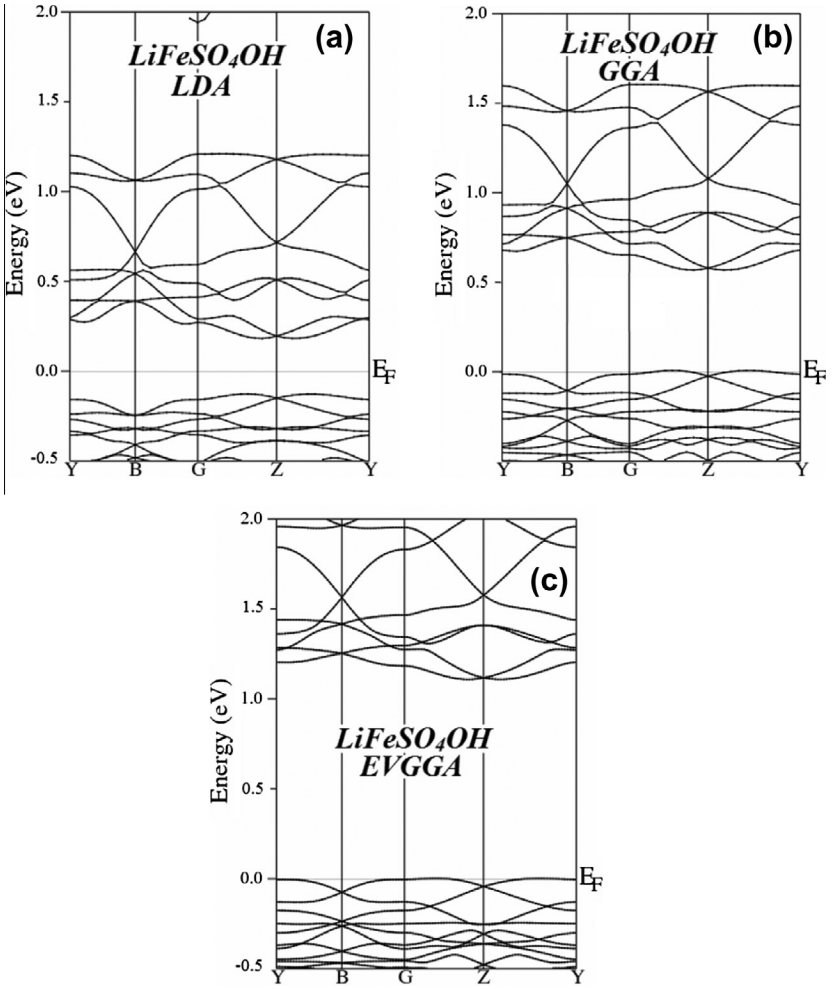

Fig. 2. Calculated band structure of $LiFeSO_4OH$ using (a) LDA (b) GGA-PBE and (c) EVGGA.

Table 2
Calculated band gap of $LiFeSO_4OH$ using (a) LDA (b) GGA and (c) EV–GGA.

Compound	LDA	GGA	EVGGA
$LiFeSO_4OH$	0.334	0.580	1.114

the difference of the charge transfer toward the O atom due to high electronegativity than Li. From these 2D contours plots one can see that the bonding nature of the compound $LiFeSO_4OH$, is mainly covalent, that leads to the conducting nature of the material.

3.3. Optical properties

From the density functional theory, we calculate the imaginary part of the complex dielectric function $\varepsilon_2(\omega)$, which can be derived by summing up the total transitions from the occupied states to unoccupied states for energies larger than those of phonons:

$$\varepsilon_2^{ij}(\omega) = \frac{Ve^2}{2\pi\hbar m^2\omega^2}\int d^3k \sum_{nn'}\langle kn|Pi|kn'\rangle \times \langle kn|Pj|kn'\rangle f_{kn}(1-f_{kn'}) \times \delta(\varepsilon_{kn'} - \varepsilon_{kn} - \hbar\omega) \quad (1)$$

Here in the above equation the term $(p_x, p_y, p_z) = p$ stands for the momentum operator, f_{kn} stands for the Fermi distribution and stands for the wave function of the crystal associated to the eigenenergy ε_{kn} with momentum vector $\vec{k}$. Since, by symmetry the investigated crystal $LiFeSO_4OH$ is monoclinic, which has several non-zero tensor components, but we will focus only on the diagonal components (ε^{xx}, ε^{yy}, ε^{zz}), which correspond to the parallel component of the electric field $E||z$ and perpendicular component of the electric field $E \perp z$ to the crystalline axis (consider c-axis).

In order to explain the effect of local density approximation (LDA), generalized gradient approximation (GGA) and Engel–Vosko GGA (EVGGA), we computed the average value of the imaginary part of the dielectric function $\varepsilon_2^{ave}(\omega)$ for the investigated compound $LiFeSO_4OH$ as illustrated in Fig. 5a. Following Fig. 5a, it is clear that EVGGA present a significant shift as compared to LDA and GGA along the entire spectral region. The shift in the calculated spectra of $\varepsilon_2^{ave}(\omega)$ is in agreement with the investigated band structure (BS) and corresponding electron density of states (DOS) of $LiFeSO_4OH$. The fundamental absorption edges are found to be at 0.03 eV, 0.16 eV and 0.64 eV for LDA, GGA and EVGGA, for $\varepsilon_2^{ave}(\omega)$ respectively, which provide a threshold for the direct optical transitions from the occupied states (valence band) to unoccupied states (conduction band). LDA and GGA underestimation in the band gape are responsible for the difference in the values of the optical absorption edges. This is mostly due to the detail that LDA and GGA are based on simple model assumptions which are not adequately tractable to reproduce sufficiently the exchange correlation (XC) energy and its charge space derivative. The EVGGA approach is better than LDA and GGA, and reproduces better exchange correlation (XC) potential.

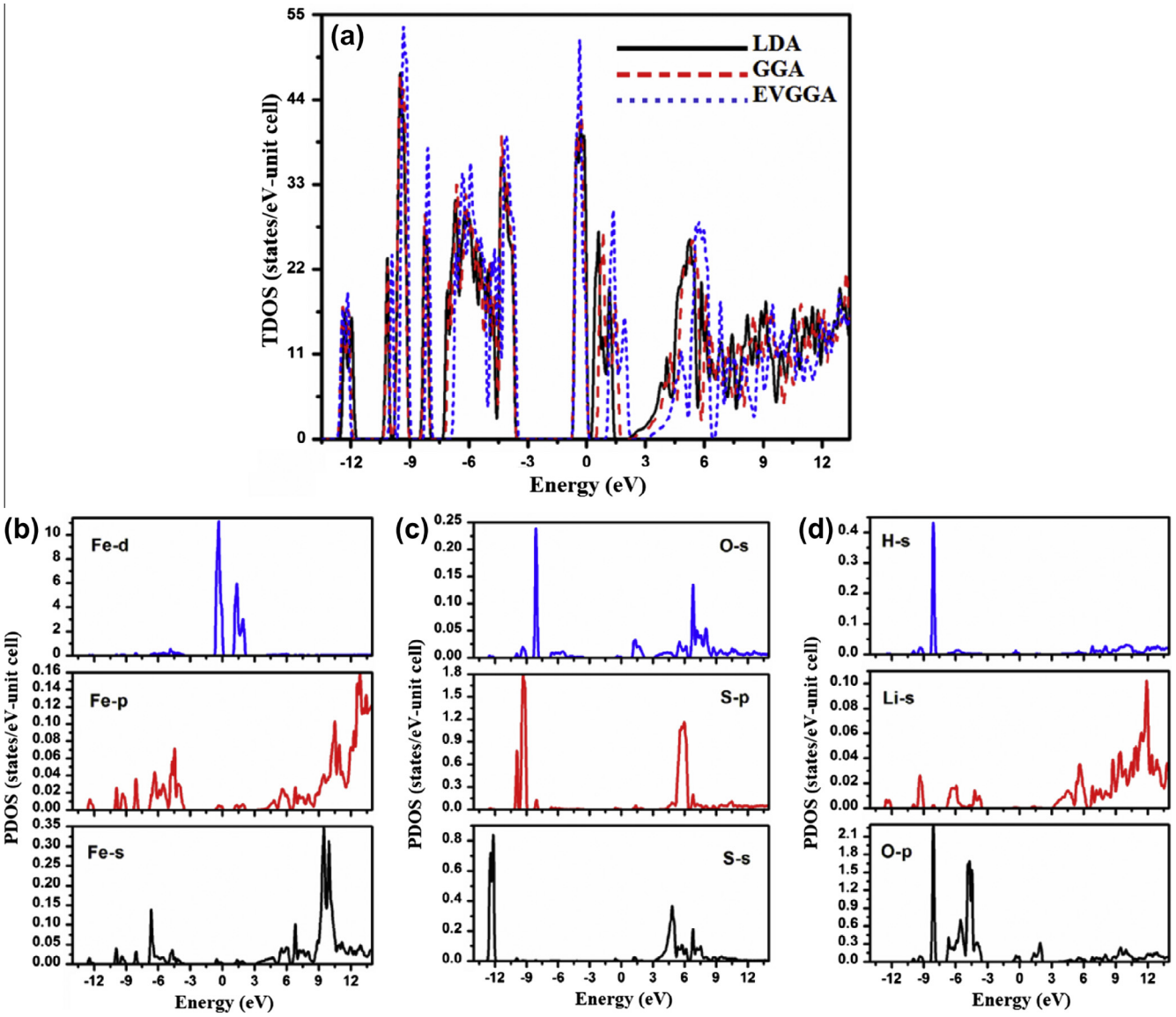

Fig. 3. Calculated total density state (DOS) and partial density of states (PDOS) of $LiFeSO_4OH$ structure.

Fig. 5b shows the imaginary part $\varepsilon_2^{xx}(\omega)$, $\varepsilon_2^{yy}(\omega)$ and $\varepsilon_2^{zz}(\omega)$ of the corresponding dielectric function $\varepsilon(\omega)$.The imaginary part of the complex dielectric function $\varepsilon_2(\omega)$ indicates small anisotropy between $\varepsilon_2^{yy}(\omega)$ and $\varepsilon_2^{zz}(\omega)$, while $\varepsilon_2^{xx}(\omega)$ exhibit significant anisotropy with $\varepsilon_2^{yy}(\omega)$ and $\varepsilon_2^{zz}(\omega)$ at the energy region between 0.0 and 3.0 eV, 5.0 and 8.0 eV and from 10.0 eV and above. In the energy range less than 1.0 eV, $\varepsilon_2(\omega)$ show high transparency and no absorption arise in this range. The first absorption edge starts from the transition of electron from Fe-3d and Fe-3p states in the VBM to O/S-2p and S-2s in CBM. In the energy range from 1.0 eV to 3.0 eV, $\varepsilon_2^{yy}(\omega)$ and $\varepsilon_2^{zz}(\omega)$ show high peaks as compared to $\varepsilon_2^{xx}(\omega)$.

In the energy range from 5.0 eV to 7.0 eV, there exist another two main structures. One can see that the three components of $\varepsilon_2(\omega)$ are contribute. The maximum value of peaks for $\varepsilon_2^{xx}(\omega)$, $\varepsilon_2^{yy}(\omega)$ and $\varepsilon_2^{zz}(\omega)$ are observed at 9.91, 9.71 and 9.86 eV respectively (Fig. 5c). These structures are belonging to the transitions from S-2p, H-2s, states to Li-2s and Fe-2s states. At higher energy beyond 12.0 eV, the compounds show high reflectivity and minute absorption.

The components and average value of the real part of the complex dielectric function $\varepsilon_1^{xx}(\omega)$, $\varepsilon_1^{yy}(\omega)$, $\varepsilon_1^{zz}(\omega)$ and $\varepsilon_1^{ave}(\omega)$ are acquired from the imaginary part of the complex dielectric tensor components by using the Kramers–Kronig dispersion relation [31,32] as displayed in Fig. 5(c and d). The calculated static values of $\varepsilon_1^{xx}(0)$, $\varepsilon_1^{yy}(0)$, $\varepsilon_1^{zz}(0)$ and $\varepsilon_1^{ave}(0)$ are presented in Table 3. Following Table 3, the values of $\varepsilon_1^{ave}(0)$ are presented for LDA, GGA and EVGGA, thus according to Ref. [33–35], smaller band gap material yield bigger static values of $\varepsilon_1(0)$, which is explained on the basis of Penn model [36] following the expression $\varepsilon(0) \approx 1 + (\hbar\omega_p/E_g)^2$. Here E_g represent the average band gap i.e. related to the real energy gape and is inversely proportional to the $\varepsilon(0)$ [37–39].

By knowing the real and imaginary parts of the complex dielectric function $\varepsilon(\omega)$ (frequency dependent), we can calculate the reflectivity $R(\omega)$, energy loss function $L(\omega)$, refractive index $n(\omega)$, extension co-efficient $K(\omega)$ and absorption co-efficient $I(\omega)$. The frequency dependence of reflectivity $R(\omega)$ is shown in Fig. 5e. There is considerable anisotropy between $R^{xx}(\omega)$, $R^{yy}(\omega)$ and $R^{zz}(\omega)$ (spectral components) along the spectral region up to 13.0 eV, except in the energy range from 8.0 eV to 9.5 eV, the three components show isotropic behavior. The reflectivity spectra consist of four main peaks. In the visible and UV regions, the reflectivity of the investigated compound show stable reflectivity about 16%.

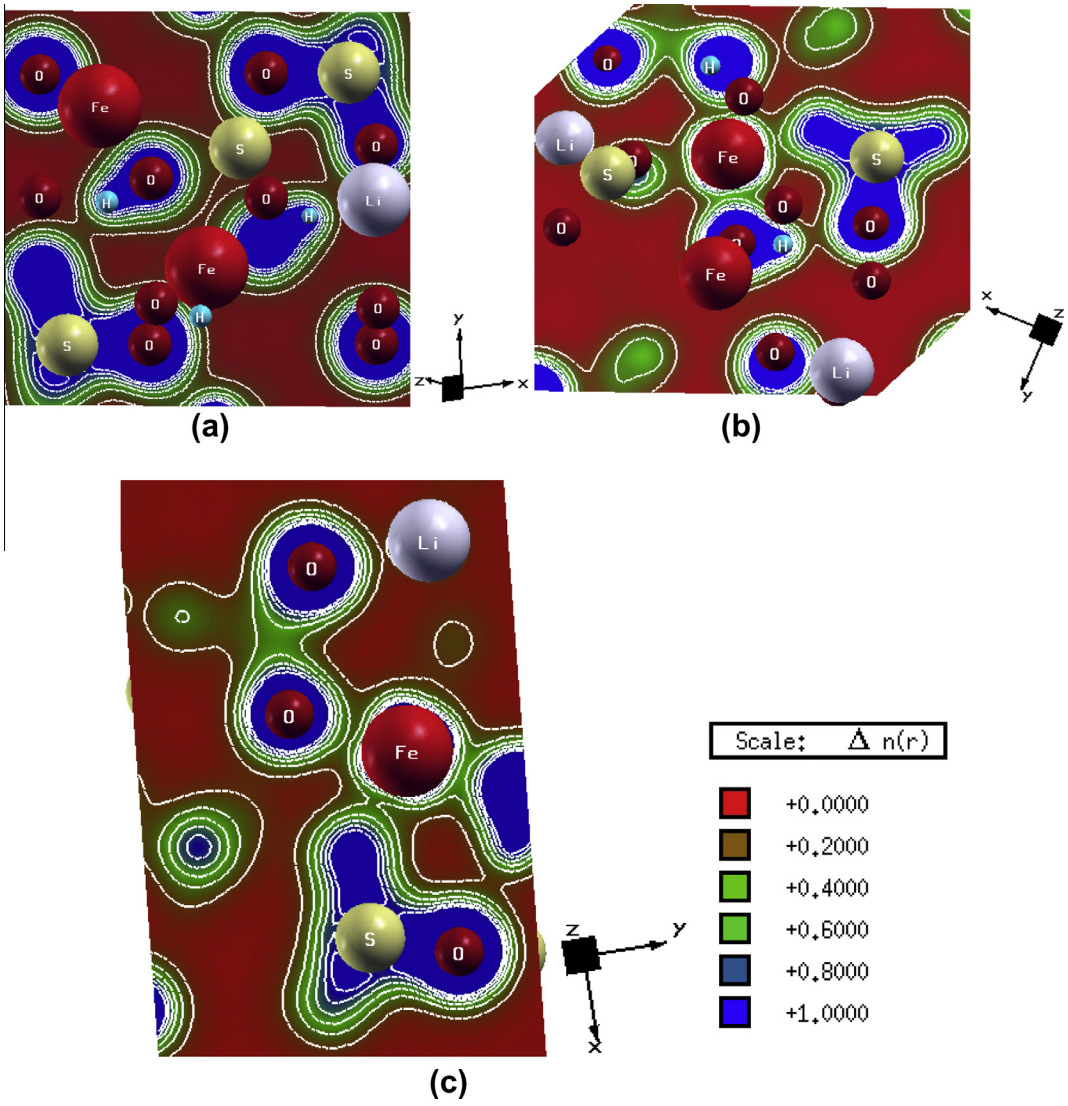

Fig. 4. Electronic space charge density distribution contour calculated with EVGGA in the (110), (100) and (100) planes of $LiFeSO_4OH$.

Following Fig. 5e all the spectral components show maximum value of reflectivity at 13.8 eV.

The calculated absorption coefficient $I(\omega)$ as a function of frequency is plotted in Fig. 5f. At lower energy range (3.0–5.0 eV), there exists isotropic behavior between $I^{xx}(\omega)$, $I^{yy}(\omega)$ and $I^{zz}(\omega)$. In the energy region between 5.0 and 9.0 eV the spectral components of absorption coefficient $I^{xx}(\omega)$, $I^{yy}(\omega)$ and $I^{zz}(\omega)$ depict small absorption peaks. At higher energy beyond 9.5 eV the absorption co-efficient $I(\omega)$ show many peaks and reaches its maximum value at energy 13.6 eV due to the excitation of phonons. It is clear that $I^{yy}(\omega)$ and $I^{zz}(\omega)$ show small anisotropic behavior but with the $I^{xx}(\omega)$ have considerable anisotropy along the whole spectral region.

We also calculate the real and imaginary part of the complex refractive index $\tilde{n}(\omega)$ along the crystallographic directions (x, y and z-axis), which can be written as [40]:

$$\tilde{n}(\omega) = n(\omega) + ik(\omega) \tag{2}$$

where $n(\omega)$ = normal refractive index and $k(\omega)$ = extension co-efficient.

The complex refractive index $\tilde{n}(\omega)$ is found from the following expression:

$$[\tilde{n}(\omega)]^2 = \varepsilon_1(\omega) + i\varepsilon_2(\omega) \tag{3}$$

Fig. 5g shows the calculated refractive index $n(\omega)$. The relation given below which correlate the static values of $n(0)$ and $\varepsilon_1(0)$ is valid at frequency ($\omega = 0$), is:

$$n(0) = \sqrt{\varepsilon_1(0)} \tag{4}$$

The calculated static values of refractive index $n(0)$ along the crystallographic axes are given in Table. 3. The average of the static values of $n(0)$ is equal to1.75. The calculated extension co-efficient $K(\omega)$ is shown in Fig. 5h. $K(\omega)$ possesses greater value along the crystalline axes at energy 13.5 eV ($K^{xx}(\omega)$), 9.8 eV ($K^{yy}(\omega)$) and 9.9 eV ($K^{zz}(\omega)$) respectively.

At last, the energy lose function $L(\omega)$ is plotted in Fig. 5i, which is obtained from the real $\varepsilon_1(\omega)$ and imaginary $\varepsilon_2(\omega)$ parts of the complex dielectric function $\varepsilon(\omega)$. It is obvious from Fig. 5i that $L^{yy}(\omega)$ and $L^{zz}(\omega)$ depict small anisotropy but have considerable anisotropy with $L^{xx}(\omega)$ along the entire spectrum ranging from 1.0 eV to 13.0 eV except from 3.0 eV to 5.0 eV and from 9.0 eV to 10.0 eV all the three components show isotropic nature. The components $L^{yy}(\omega)$ and $L^{zz}(\omega)$ of energy loss function posses larger values at 2.38 eV (0.332) for $L^{yy}(\omega)$ and at 2.40 eV (0.65) for $L^{zz}(\omega)$, while the x-component of energy loss function $L^{xx}(\omega)$ has the lowest energy loss value at 1.69 eV (0.05). There are some other peaks appear for the energy loss function $L(\omega)$ in the energy range from

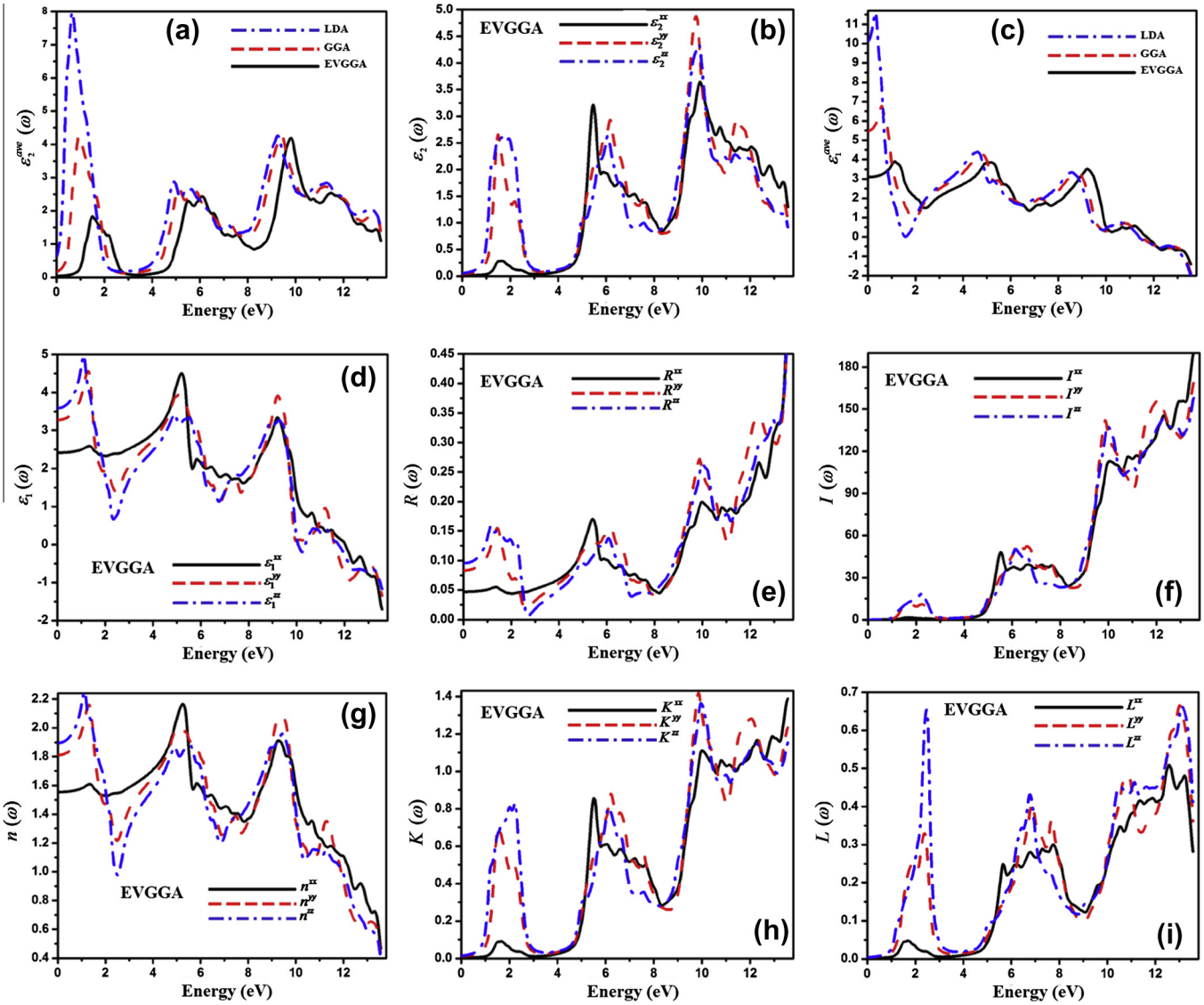

Fig. 5. Calculated real and imaginary part of dielectric function, reflectivity, energy loss function, refractive index and absorption coefficient of $LiFeSO_4OH$ using EVGGA.

Table 3
Calculated value of $\varepsilon_1^{ave}(0)$, $\varepsilon_1^{xx}(0)$, $\varepsilon_1^{yy}(0)$, $\varepsilon_1^{zz}(0)$, $n^{xx}(0)$, $n^{yy}(0)$, $n^{zz}(0)$.

	$\varepsilon_1^{ave}(0)$	$\varepsilon_1^{xx}(0)$	$\varepsilon_1^{yy}(0)$	$\varepsilon_1^{zz}(0)$	$n^{xx}(0)$	$n^{yy}(0)$	$n^{zz}(0)$
LDA	10.15	3.56	10.60	16.28	–	–	–
GGA	5.47	3.01	5.92	7.46	–	–	–
EVGGA	3.09	2.41	3.27	3.59	1.55	1.81	1.89

5.0 eV to 13.6 eV along the entire spectral region, and all spectral components of energy loss function ($L^{xx}(\omega)$, $L^{yy}(\omega)$ and $L^{zz}(\omega)$) reaches its maximum value at 12.6 eV ($L^{xx}(\omega) = 0.51$), 13.04 eV ($L^{yy}(\omega) = 0.666$) and at 13.09 eV ($L^{zz}(\omega) = 0.664$) respectively. All these peaks correspond to the plasmon peaks in the energy loss $L(\omega)$ spectra for the identical polarization.

3.4. Thermoelectric properties

We also investigated the electronic transport properties, like electrical conductivity σ, thermal conductivity κ, Seebeck co-efficient S and power factor $S^2\sigma$ as a function of carrier concentration n at different temperatures (T) of $LiFeSO_4OH$, which is based on the band structure using the Boltzmann theory. It is very simple execution because it needs only one electronic structure calculation per compound to carry out the electronic transport coefficients [41,42].

In Fig. 6a average value of electrical conductivity σ^{ave}/τ is plotted as a function of carrier concentration at different temperatures from 300 K to 750 K. It is clear from Fig. 6a that the electrical conductivity σ^{ave}/τ exhibits strong variation due to carrier concentration (n) and also with the temperature (T). The total carrier concentration is defined as the difference between the hole and the electron concentration. While the electron and holes carrier concentration are define as:

$$P = \frac{2}{\Omega}\int_{BZ}\int_{VB}[1 - f_0(T,\varepsilon,\mu)]d\varepsilon \tag{5}$$

$$n = \frac{2}{\Omega}\int_{BZ}\int_{CB} f_0(T,\varepsilon,\mu)d\varepsilon \tag{6}$$

In the above equation, the integral is performed over the Brillouin Zone (BZ) as well as over conduction band (CB) for electrons (n) or valence band (VB) for holes (p). The electrical conductivity σ^{ave}/τ shows anisotropy as shown in Fig. 6a. Following Fig. 6a, the anisotropy of electrical conductivity σ^{ave}/τ of n-type doping

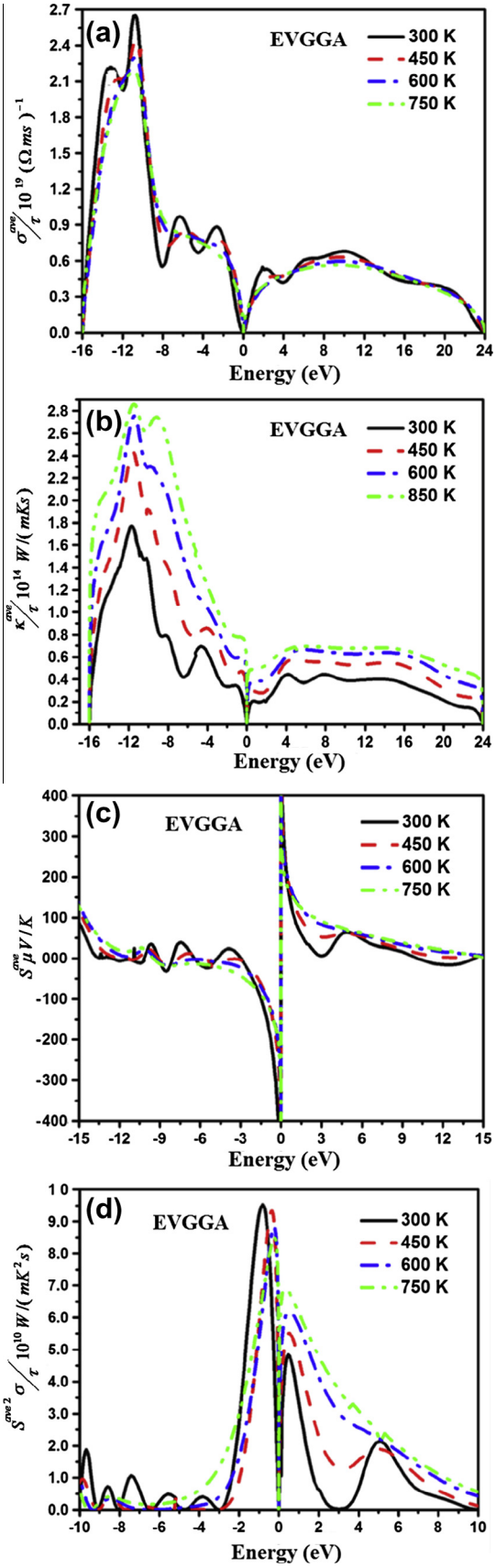

Fig. 6. Calculated transport coefficients of $LiFeSO_4OH$ as a function of carrier concentration: electrical and Thermal conductivity, Seebeck coefficient and power factor.

is greatly influenced by the greater carrier concentration. The σ^{ave}/τ along the z-direction indicate better value as compared to the x and y directions. One can also see from Fig. 6a that anisotropy of σ^{ave}/τ also increases due to the increase in the temperature ranging from 300 K to 750 K. For n-type doping, the anisotropy of σ^{ave}/τ is greater as compared to the p-type doping is shown in Fig. 6a. In spite of n-type or p-type doping, electrical conductivities boost with increasing carrier concentration, which is in accord with electrical conductivity proportional to the carrier concentration.

Fig. 6b shows that the thermal conductivity κ^{ave}/τ as a function of carrier concentration at different value of temperatures (T). It is clear from Fig. 6b that at 300 K thermal conductivity κ^{ave}/τ of Li_2FeSO_4OH is smaller than that of κ^{ave}/τ at other temperature (450 K, 600 K, and 750 K). The smaller value of thermal conductivity κ^{ave}/τ of the corresponding compound at 300 K means that it is good thermoelectric material. The thermal conductivity κ^{ave}/τ increases due to the increase in temperature from 300 K to 750 K at the same carrier concentration as displayed in Fig. 6b. Furthermore, thermal conductivity κ^{ave}/τ shows greater anisotropy in n-type doping as compared to p-type doping due to which the electron can easily flow than that of holes. At high temperature, we ignore lattice thermal conductivity κ_l as compared to the thermal conductivity of electron κ_e i.e. κ is mainly due to the κ_e.

The Seebeck co-efficient S^{ave}/τ is plotted versus carrier concentration at different temperatures from 300 K to 750 K as shown in Fig. 6c. The Seebeck coefficient S^{ave}/τ is lying in the range of -400 μV/K to 400 μV/K, which is comparatively best i.e. other familiar thermoelectric materials [43–47]. We observed that both n-type and p-type possess the same contribution to the Seebeck co-efficient S^{ave}/τ with the same carrier concentration at the same temperature, which is attributed to the DOS structure. The bipolar conduction also takes place in the entire range of temperature because of small band gap. Due to the increase in the temperature from 300 K to 750 K, the Seebeck co-efficient S^{ave}/τ decreases at the same carrier concentration.

We calculate the power factor $S^{ave^2}\sigma$ from the calculated Seebeck co-efficient S^{ave} and electrical conductivity σ^{ave}, which is also plotted as a function of carrier concentration at different temperature from 300 K to 750 K is shown in Fig. 6d. The power factor $S^{ave^2}\sigma$ for n-type doping exhibits greater anisotropy than that of p-type doping that is mainly due to the anisotropy of electrical conductivity σ^{ave}/τ. Hence, the n-type doping of $LiFeSO_4OH$ indicate enhanced thermoelectric properties as compared to p-type doping and display greater $S^{ave^2}\sigma$ along the z-direction, which is also good for thermoelectric properties. The power factors $S^{ave^2}\sigma$ of n-type as well as of p-type doping is very appreciable and in comparison to other renowned thermoelectric materials [43–45,47].

4. Conclusions

The purpose of this research work is to study the electronic structure and optical properties of the layered polyanionic hydroxysulfate $LiFeSO_4OH$ using density functional theory (DFT). From the calculated result of band structure, it is found that $LiFeSO_4OH$ is a direct band gap semiconductor. The electronic charge density is obtained, which present the covalent bonds between S, O, and H and polar covalent bond between O and Fe. All the frequency dependent optical properties are investigated, which suggest that the investigated compound has preeminent photoelectric properties and can be used in opto-electronic device. Using the Boltzmann transport calculation, we also analyze the thermoelectric properties as a function of carrier concentrations, of heavily electron doped $LiFeSO_4OH$ at different temperatures ranging

from 300 K to 750 K. The value of the calculated Seebeck co-efficient is large as 400 μV/K, which is enormously rare and report that $LiFeSO_4OH$ is excellent thermoelectric material. The calculated value of the power factor is also appreciable in these ranges of temperature and carrier concentration.

Acknowledgement

This result was developed within the CENTEM project, reg. No. CZ.1.05/2.1.00/03.0088, co-funded by the ERDF as part of the Ministry of Education, Youth and Sports OP RDI program. School of Material Engineering, Malaysia University of Perlis, Malaysia.

References

[1] M.M. Thackeray, C.S. Johnson, J.T. Vaughey, N. Li, S.A. Hackney, J. Mater. Chem. 15 (2005) 2257.
[2] A.K. Padhi, K.S. Nanjundaswamy, J.B. Goodenough, J. Electrochem. Soc. 144 (1997) 1188.
[3] A. Nyten, A. Abouimrane, M. Armand, T. Gustafsson, J.O. Thomas, Electrochem. Commun. 7 (2005) 156.
[4] S. Nishimura, M. Nakamura, R. Natsui, A. Yamada, J. Am. Chem. Soc. 132 (2010) 13596.
[5] A. Yamada, N. Iwane, Y. Harada, S. Nishimura, Y. Koyama, I. Tanaka, Adv. Mater. 22 (2010) 3583.
[6] A.K. Padhi, V. Manivannan, J.B. Goodenough, J. Electrochem. Soc. 145 (1998) 1518.
[7] N. Recham, J.N. Chotard, L. Dupont, C. Delacourt, W. Walker, M. Armand, J.M. Tarascon, Nat. Mater. 9 (2010) 68.
[8] N. Recham, G. Rousse, M.T. Sougrati, J.N. Chotard, C. Frayret, M. Sathiya, B.C. Melot, J.C. Jumas, J.M. Tarascon, Chem. Mater. 24 (2012) 4363.
[9] B.C. Melot, G. Rousse, J.N. Chotard, M.C. Kemei, J. Rodriguez-Carvajal, J.M. Tarascon, Phys. Rev. B 85 (2012) 4415.
[10] M. Ati, M.T. Sougrati, G. Rousse, N. Recham, M.L. Doublet, J.C. Jumas, J.M. Tarascon, Chem. Mater. 24 (2012) 1472.
[11] M. Ati, M. Sathiya, S. Boulineau, M. Reynaud, A. Abakumov, G. Rousse, B. Melot, G. Van Tendeloo, J.M. Tarascon, J. Am. Chem. Soc. 134 (2012) 18380.
[12] B.C. Melot, G. Rousse, J.N. Chotard, M. Ati, J. Rodriguez- Carvajal, M.C. Kemei, J.M. Tarascon, Chem. Mater. 23 (2011) 2922.
[13] P. Barpanda, M. Ati, B.C. Melot, G. Rousse, J.N. Chotard, M.L. Doublet, M.T. Sougrati, S.A. Corr, J.C. Jumas, J.M. Tarascon, Nat. Mater. 10 (2011) 772.
[14] M. Ati, B.C. Melot, G. Rousse, J.N. Chotard, P. Barpanda, J.M. Tarascon, Angew. Chem. Int. Ed. 50 (2011) 10574.
[15] M. Ati, B.C. Melot, J.N. Chotard, G. Rousse, M. Reynaud, J.M. Tarascon, Electrochem. Commun. 13 (2011) 1280.
[16] Chinmayee V. Subban, Mohamed Ati, Gwenaëlle Rousse, Artem M. Abakumov, Gustaaf Van Tendeloo, Raphaël Janot, Jean-Marie Tarascon, J. Am. Chem. Soc. 135 (2013) 3653–3661.
[17] E. Engel, S.H. Vosko, Phys. Rev. B 47 (1993) 13164;
E. Engel, S.H. Vosko, Phys. Rev. B 50 (1994) 10498.
[18] L. Thomas, Proc. Cambridge Philos. Soc. 23 (1927) 542.
[19] E. Fermi, Z. Phys. 48 (1928) 73.
[20] P. Hohenberg, W. Kohn, Phys. Rev. 136 (1964) B864.
[21] K. Schwarz, P. Blaha, G.K.H. Madsen, Comput. Phys. Commun. 147 (2002) 71.
[22] D. Koelling, G. Arbman, J. Phys. F: Met. Phys. 5 (1975) 2041.
[23] O.K. Andersen, Phys. Rev. B 12 (1975) 3060.
[24] O. Jepsen, J. Madsen, O.K. Andersen, Phys. Rev. B 26 (1982) 2790.
[25] M. Weinert, E. Wimmer, A. Freeman, Phys. Rev. B 26 (1982) 4571.
[26] H. Jansen, A. Freeman, Phys. Rev. B 30 (1984) 561.
[27] L. Mattheiss, D. Hamann, Phys. Rev. B 33 (1986) 823.
[28] S. Cottenier, Density functional theory and the family of (L)APW-methods: A Step-by-Step Introduction Instituut voor Kern-en Stralingsfysica, K.U. Leuven, Belgium, 2002.
[29] J.P. Perdew, Y. Wang, Phys. Rev. B 45 (1992) 13244.
[30] J.P. Perdew, J.A. Chevary, S.H. Vosko, K.A. Jackson, M.R. Pederson, D.J. Singh, C. Fiolhais, Phys. Rev. B 46 (1992) 6671.
[31] A.H. Reshak, Saleem Ayaz Khan, Comput. Mater. Sci. 78 (2013) 91–97.
[32] H. Tributsch, Z. Naturforsch, A 32A (1977) 972.
[33] A.H. Reshak, Int. J. Electrochem. Sci. 8 (2013) 9371.
[34] S.J. Asadabadi, Phys. Rev. B 75 (2007) 205130.
[35] S.A. Khan, A.H. Reshak, Int. J. Electrochem. Sci. 8 (2013). 9459–947.
[36] D.R. Penn, Phys. Rev. B 128 (1962) 2093.
[37] A.H. Reshak, H. Kamarudin, S. Auluck, J. Mater. Sci. 48 (2013) 1955–1965.
[38] A. Manzar, G. Murtaza, R. Khenata, S. Muhammad, Hayatullah, Chin. Phys. Lett. 30 (2013) 067401.
[39] Hayatullah, G. Murtaza, R. Khenata, S. Mohammad, S. Naeem, M.N. Khalid, A. Manzar, Physica B 420 (2013) 15–23.
[40] L. Makinistian et al., Phys. Rev. B 81 (2010) 075217.
[41] C. Stiewe, L. Bertini, M. Toprak, M. Christensen, D. Platzek, S. Williams, C. Gatti, E. Muller, B.B. Iversen, M. Muhammed, M. Rowe, J. Appl. Phys. 97 (2005) 044317.
[42] L. Chaput, P. Pecheur, J. Tobola, H. Scherrer, Phys. Rev. B 72 (2005) 085126.
[43] J.P. Heremans, V. Jovovic, E.S. Toberer, A. Saramat, K. Kurosaki, A. Charoenphakdee, S. Yamanaka, G.J. Snyder, Science 321 (2008) 554–557.
[44] J.S. Rhyee, K.H. Lee, S.M. Lee, E. Cho, S.I. Kim, E. Lee, Y.S. Kwon, J.H. Shim, G. Kotliar, Nature 459 (2009) 965–968.
[45] D. Parker, D.J. Singh, J. Appl. Phys. 108 (2010) 083712.
[46] A.N. Qiu, L.T. Zhang, J.S. Wu, Phys. Rev. B 81 (2010) 035203.
[47] D.Y. Chung, T.P. Hogan, M. Rocci-Lane, P. Brazis, J.R. Ireland, C.R. Kannewurf, M. Bastea, C. Uher, M.G. Kanatzidis, J. Am. Chem. Soc. 126 (2004) 6414–6428.